American Research Journal of Physics **Original Article**
ISSN 2380-5714 **Volume 1, Issue 2, 2015**

Transparent and Conducting $TiO_2:Nb$ Thin Films Prepared by Spray Pyrolysis Technique

Maxwell J. Mageto[1,4], C.M. Maghanga[2], M. Mwamburi[3], Hassan Jafri[4]

[1]Department of Physics, Masinde Muliro University of Science and Technology, P.O. Box 190, 50100, Kakamega, Kenya.
[2]Department of Physics, Kabarak University, P.o. Private Bag, Nakuru, Kenya.
[3]Department of Physics, University of Eldoret, P.o. Box 1125, Eldoret, Kenya.
[4]Ångström Laboratory, Uppsala University, P.O. Box 524, SE.75120 Uppsala, Sweden.

Abstract: To date, only sputtering and pulsed laser deposition (PLD) techniques have been employed successfully to fabricate highly conducting and transparent TiO_2:Nb (TNO) films. In this article, we demonstrate that transparent and conducting $TiO_2:Nb$ films can be made by the spray pyrolysis technique. The films were deposited on Corning 7059 glass substrates at $500 \pm 15^{\circ}C$ using an alcoholic precursor solution consisting of titanium (iv) isopropoxide and $NbCl_5$. The influence of increasing Nb concentration on the electrical, optical and structural properties was investigated. The minimum resistivity, 3.36×10^{-3} Ω cm, for $Ti_{1-x}Nb_xO_2$ film (x = 0.15) was obtained after 1 hour post deposition annealing in hydrogen atmosphere at 500°C. The x-ray diffraction of hydrogen annealed films showed a polycrystalline anatase (004)-oriented phase without any second phases. The optical band gap for undoped and doped films lay in the range 3.38 – 3.47 eV. Using dispersion analysis, optical constants were determined from spectro-photometric measurements for films on glass.

Keywords: Spray Pyrolysis; Titanium dioxide; Transparent conductor; Doping.

I. INTRODUCTION

Titanium dioxide (TiO_2) thin films have been investigated extensively in recent years owing to their potential applications in areas such as photo-catalysis [1], electro-chromism [2], solar cells [3], self cleaning windows[2], gas sensors[2], optical wave-guides[3] etc. Transparent conducting oxides (TCOs) [2] such as fluorine doped tin oxide (FTO), tin doped indium oxide (ITO), aluminum doped zinc oxide (AZO) have attracted much attention both in fundamental research and device applications such as flat panel displays (FPDs), touch panels, light emitting diodes (LEDs), and Si-based solar cells [4]. Since 2005, niobium doped titanium oxide (TNO) has joined the conventional class of TCOs mentioned above [2].

Anatase undoped TiO_2 films have been deposited by various techniques [4,5] including sputtering, pulsed laser deposition (PLD), chemical vapour deposition (CVD)[6], sol-gel[7,8] and spray pyrolysis[9]. To date, only sputtering [10,11 ,12 ,13 ,14] and pulsed laser deposition (PLD) [15,16 ,17 ,18 ,19] techniques have been employed successfully to fabricate highly conducting and transparent TiO_2:Nb (TNO) films [4]. TNO films with resistivity 2 - 3×10^{-4} Ω cm at do pant concentrations of 3 - 6 at. % have been achieved by PLD [4,18] although unexpectedly, resistivity remained on the order of 10^{-4} Ω cm for do pant concentrations as high as 20 at. % [18]. These highly conductive TNO films are typically degenerate semiconductors: the do pant Nb atoms exist as Nb^{5+} ions, and release conduction electrons with high efficiency [4]. The ionic radius of Nb^{5+} is 0.64 Å. This is close to that of Ti^{4+} radius (0.60 Å). Thus, Nb is supposed to be substituted for Ti, in the lattice making the doped TiO_2 a n-type semiconductor.

In this paper, we report for the first time, the fabrication of low resistivity and transparent TNO films made by the low cost, vacuum-free spray pyrolysis combined with post deposition annealing. The influence of increasing Nb concentration on the electrical, optical and structural properties was investigated. This paper is organized as follows: Section 2 describes the experimental setup for the preparation of the films including sample preparation, post

[1] *Corresponding Author: jmmageto@yahoo.com*

deposition annealing and characterization techniques. Section 3 is devoted to experimental results including chemical composition, structural, optical and electrical properties. An analysis of the optical data is given; results are reported for optical constants and band gaps. This Section also covers film characterization with x-ray diffraction and scanning electron microscopy. Section 4, summarizes the main results.

II. EXPERIMENTAL

2.1. Sample Preparation

Substrates were cleaned in an ultrasonic bath containing soap detergent for 15 minutes and the procedure was repeated using pure ethanol instead of detergent. Undoped and niobium-doped titanium oxide films were deposited onto pre-cleaned 0.5 mm thick $2.5\times 5\ cm^2$ Corning 7059 glass and silicon substrates by spray pyrolysis at a substrate temperature of $500\pm 15^{\circ}C$. The detailed description of the spray pyrolysis reactor is given elsewhere [20]. The deposition apparatus consists of a spray chamber, hot plate (substrate heater), temperature controller, atomizer (spray nozzle) of diameter ~1mm, input gas valve, gas compressor, gas flow meter, conduit tube, pressure gauge.

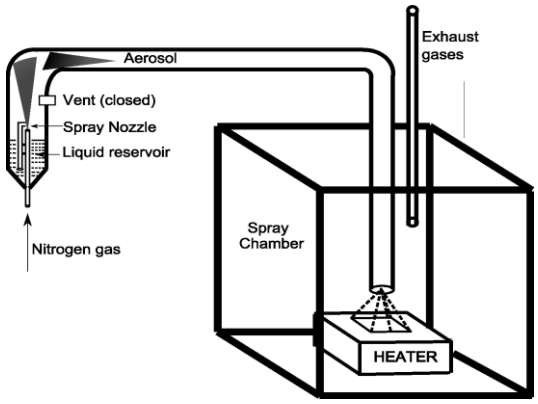

Fig1. *Spray Pyrolysis experimental setup.*

The schematic view of the in-house-made spray pyrolysis system is depicted in

Fig1. The setup works inside a fume chamber whose air venting velocity is 0.51 m/s.The undoped TiO_2 films were produced from a precursor solution consisting of titanium (iv) isopropoxide (TPT) (97% Alfa Aesar) prepared by mixing 34.7g of TPT with 54ml of 2,4-pentanedione (99% Alfa Aesar). They react to form Titanium diisopropoxide bis(acetylacetonate) and isopropanol [21]. This reaction is exothermic meaning that the flask gets hot. After cooling, the resulting solution was diluted with 810 ml pure ethanol and 10ml of 35% HCl under standard atmospheric conditions and then stirred at 60rpm for 5 hours at room temperature. During this stirring step, plastic wrap was used to cover the top of the beaker to prevent reaction with humidity. The resulting solution (labeled T) was divided into several portions each of 200 ml per beaker. Nb - doped TiO_2 films were prepared from solutions (labeled N) of (28.4g, 0.11 mol) Niobium (V) Chloride, $NbCl_5$,(99% Alfa Aesar) dissolved in 500 ml pure ethanol as well as 10ml of acetic acid, stirred as above and certain different amounts of this solution N added to each of the 200 ml of solution T. Since solution N was responsible for the introduction of do pant, the amount of $NbCl_5$ in the solution mixture of T and N was based on the required doping level. The mixture was also stirred as stated above for 30 minutes.

The spraying parameters were as follows: substrate temperature of $500\pm 15^{\circ}C$ was monitored with a thermocouple fixed 1 mm deep in the interior of the substrate holder, directly under the substrate position. Carrier-gas: Nitrogen, Carrier-gas pressure: 2.1 bar, flow rate of solution 7ml/min, nozzle-to-substrate distance: 65 cm horizontally and 40 cm vertically. To prevent rapid cooling of the hot plate temperature, spraying was done in short bursts.

2.2. Postdepositionannealing

After recording their transmittance, reflectance and x-ray diffraction (XRD) spectra, the sprayed samples were annealed in hydrogen ambient at a pressure of 1atm at heating ramp speed of 4°/min with a dwell time of 1 hour at a temperature of 500°C and thereafter cooling at a ramp speed of 4.4°/min, translating to a total of 4.8 hours.

2.3. Sample characterization

The crystal structure and phase characterization were determined using a Siemens D5000 X-ray diffract meter (XRD). The glazing incident angle was 1^0 in parallel beam geometry with the diffraction angle, 2θ, between 20^0 and 70^0. The wavelength, λ, of the CuK_α radiation was 1.540598 Å..A high resolution LEO 1550 Scanning Electron Microscope (SEM) with a field emission gun was used to examine grain size, surface and cross-sectional morphologies for different concentrations of Nb in the doped samples on silicon substrates. The elemental chemical compositions of the TiO_2: Nb films deposited on Si substrates were determined by Energy Dispersive X-ray Spectroscopy (EDS).

The transmittance and reflectance measurements were done at near normal angle of incidence in the solar wavelength range from 0.3 to 2.5 μm on a Perkin-Elmer Lamda 900 UV/VIS/NIR double beam spectrophotometer equipped with an integrating sphere. A barium sulphate film served as reflectance standard.

Thickness d, of the as-deposited and hydrogen annealed samples prepared with different Nb doping concentrations were estimated using the number of interference fringes, from the equation [[21]].

$$d = \frac{\lambda_1 \lambda_2}{2(\lambda_1 n_2 - \lambda_2 n_1)} \tag{1}$$

Where n_1 and n_2 are refractive indices at two adjacent maxima (or minima) at λ_1 and λ_2 respectively and the refractive index, n was determined as described by Swanepoel [22].

$$n = \sqrt{N + \sqrt{N^2 - S^2}} \tag{2}$$

Where

$$N = 2S\frac{T_M - T_m}{T_M T_m} + \frac{S^2 + 1}{2} \tag{3}$$

Here S denotes the refractive index of the substrate, T_M and T_m represents the maximum and minimum transmittance envelopes at the fringes.

The estimated thickness was verified by fitting the experimental spectral data to theoretical spectral data based on dispersion analysis using the SCOUT software [23] in the wavelength range 0.3 - 2.5 μm and also from SEM cross sections. The thicknesses obtained from the three different methods agree within a discrepancy of not more than 5% and are indicated below XRD spectra.

Dispersion analysis using a model for dielectric susceptibility of the film consisting of two parts: Drude [24] and Kim terms [25] was used to simulate the measured reflectance and transmittance. Drude free electron model accounts for intraband transitions of the conduction electrons which contribute to the optical properties. This model has two adjustable parameters: plasma frequency, Ω_p and damping constant, γ. The plasma frequency is proportional to the square root of the carrier density; the damping constant is proportional to the inverse of the mobility. The Drude dielectric susceptibility χ_{Drude}, expressed as a function of frequency ω, is given as [24]

$$\chi_{Drude}(\omega) = \frac{\Omega_p^2}{\omega^2 + i\omega\gamma} \tag{4}$$

The one oscillator contribution developed by Kim contains four adjustable parameters: Ω_{TO} resonance frequency, Ω_p oscillator strength, Ω_τ damping constant, and the so called Gauss–Lorentz-switch constant σ. σ may vary between zero and infinity. For σ = 0, a Gaussian line shape is achieved. A large value of σ (larger than 5) leads to a Lorentzian line shape. The Kim oscillator models the weak broad interbank absorption in the measured wavelength range. The interbank dielectric susceptibility described by Kim is given by [25];

$$\chi_{Kim,Oscillator} = \frac{\Omega_p^2}{\Omega_{TO}^2 - \omega^2 - i\omega\tau(\omega)} \tag{5}$$

Model parameters were determined from best fits between computed and experimental data using Scout software [23]. The best fit directly gave the optical constants of the film being studied as well as film thickness.

Where

$$\tau(\omega) = \Omega_\tau \exp\left[-\frac{1}{1+\sigma^2}\left(\frac{\omega-\Omega_{TO}}{\Omega_\tau}\right)^2\right] \quad (5)$$

The sheet resistance of the thin films was determined by a two-point square probe with 8 point electrodes, having Au tips in a linear arrangement and touching the coated surface. Since the two-point probe had equal length and width, resistance per unit square was obtained. By measuring the sheet resistance, R_s and the average thickness, t, of the films, the electrical resistivity, ρ or conductivity, σ of the samples was calculated using the following relation.

$$\rho = \frac{1}{\sigma} = R_s\, t \quad \textbf{(6)}$$

Temperature dependent electrical resistivity measurements were done in the temperature range 10K to 300K in a physical property measurement system (PPMS-6000, quantum design) using the standard four-probe method.

III. Results And Discussion

3.1. Composition

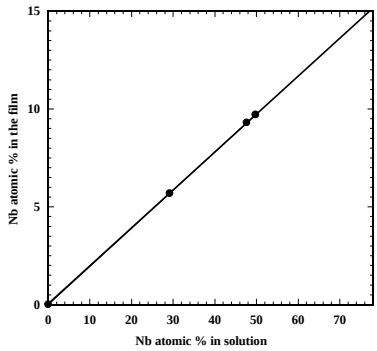

Fig2. *Nb at. % in solution (calculated) versus Nb at. % as determined from EDS*

Energy dispersive spectroscopy (EDS) was used to measure the percentage of niobium in the films. Fig shows the niobium concentration in the film as a function of chemical solution concentration for films deposited under similar conditions. The composition of the as deposited $TiO_2:Nb$ films were determined using Silicon substrates. The experimentally determined composition was proportional to the Nb content in the solution, as shown in Fig. This difference is attributed to low efficiency and a high consumption of chemical [26] due to the large separation between the nozzle and substrate to allow vaporization of the solution.

3.2. Structural Studies

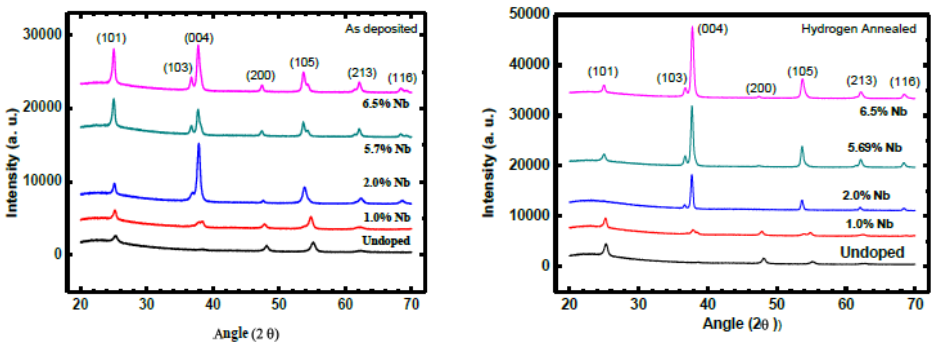

Fig3. *XRD pattern of undoped and Nb-doped* TiO_2 *films on Corning 7059 glass substrates before and after post deposition annealing in hydrogen at 500°C Thickness of each film was 600 ± 10 nm.*

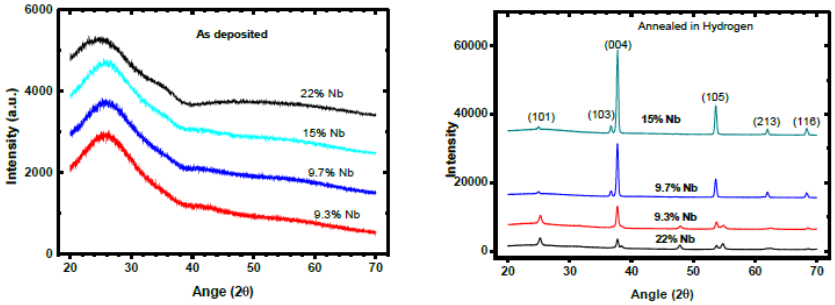

Fig4. *XRD pattern of undoped and Nb-doped* TiO_2 *films on Corning 7059 glass substrates at before and after post deposition annealing in hydrogen at 500°C Thickness of each film 336 ± 6 nm*

Fig shows the XRD patterns of the undoped and Nb doped (low Nb concentrations) polycrystalline titanium oxide films on Corning 7059 glass substrates before and after post annealing. The peaks in the spectra are identified as originating from reflections from the (101), (103), (004), (200), (105) planes of polycrystalline anatase titanium oxide. No peaks from starting materials or any residual species were found in the spectra, confirming the proper phase formation of the materials. Before annealing, the (101) peak increases with increasing Nb-doping, but after post annealing the peak is suppressed.

Fig shows the XRD patterns of Nb doped (high Nb concentrations) amorphous and polycrystalline titanium oxide films on Corning 7059 glass substrates before and after post annealing respectively. Note that as Nb concentration was increased to 9.3 at. % Nb, the films turned from crystalline to amorphous structure before annealing. After post annealing in hydrogen, the films crystallized. The intensity of the (004) peak increased remarkably as the Nb concentration was increased to 15 at. % Nb, as shown in Fig

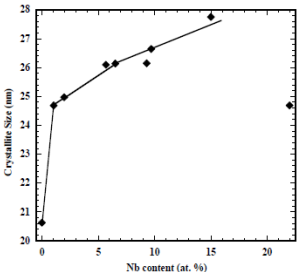

Fig5.*Variation of grain size for* $TiO_2:Nb$ *films annealed at* $500^0 C$ *in hydrogen as a function of doping concentration*

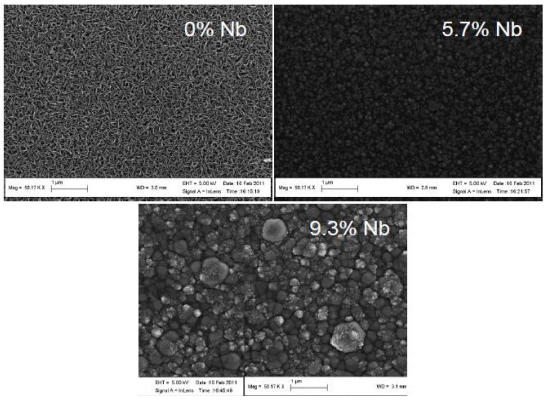

Fig6.*SEM image of films on silicon substrates as deposited (a) Undoped film (b) 5.7% Nb doped (c) 9.3% Nb doped* TiO_2

The effective grain size was determined from the full-width at half-maximum (FWHM) of the x-ray peak of the (004) plane using the well known Debye-Scherer formula, i.e.

$$D = \frac{0.9\,\lambda}{L\cos\theta} \tag{7}$$

Where L is the diameter of the crystallites forming the film, λ is the wavelength of the x-ray line, and D is the FWHM of the XRD peak. As displayed in Fig, for samples post annealed in hydrogen atmosphere at $500\,^{0}C$ for 1 hour, the estimated crystallite size increased with increasing Nb content up to 15 at. %.

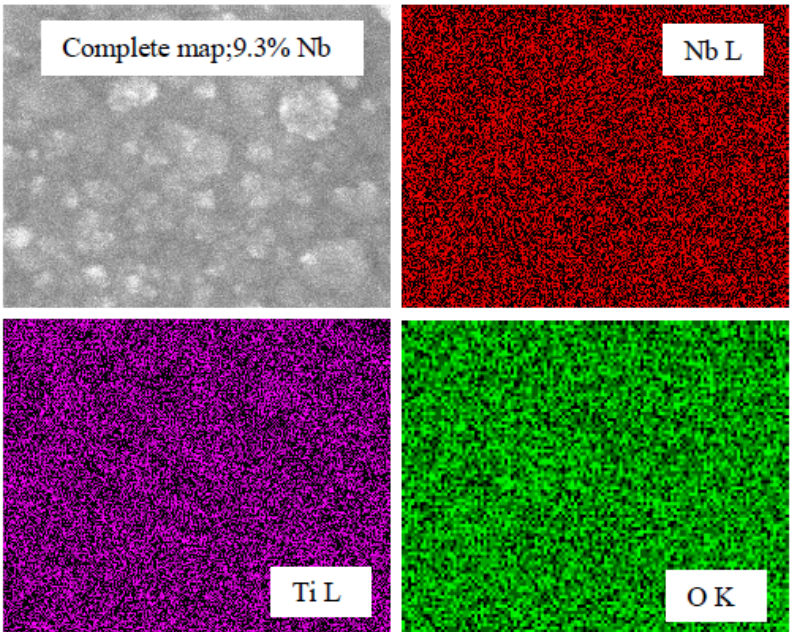

Fig7.*Elemental chemical mapping for 9.3 at % Nb doped* TiO_2

From the SEM observations in **Error! Reference source not found.**, it can be concluded that the average particle size of undoped titanium oxide is 70-150 nm. For Nb-doped titanium oxide, the particle size is larger in Nb-containing samples and the homogeneity is good as evidenced from the elemental chemical mapping Figure 7.

3.3. Optical studies

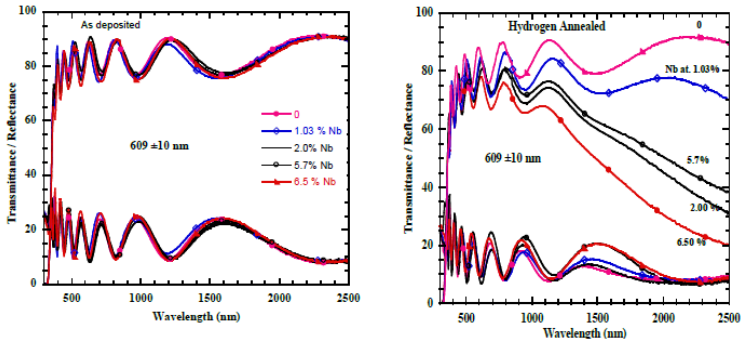

Fig8. *Experimental Spectral Transmittance and Reflectance of undoped and Nb-doped titanium oxide films prepared at 500 ± 15°C before and after post-annealing in Hydrogen atmosphere at 500°C for 1 hour (low Nb concentrations). Thickness of films was 609 ± 10 nm.*

In order to compare the transparency of hydrogen annealed $TiO_2:Nb$ thin films with various Nb-doping levels, their optical spectra in the UV-VIS–NIR region were measured. The optical transparency of $TiO_2:Nb$ thin films for

various Nb-doping levels is shown in Fig. The transparency at 540 nm decreased with increasing Nb doping concentration. Near the infrared wavelength range, the transparency decrease with increasing Nb doping became much more pronounced for the hydrogen annealed films only.

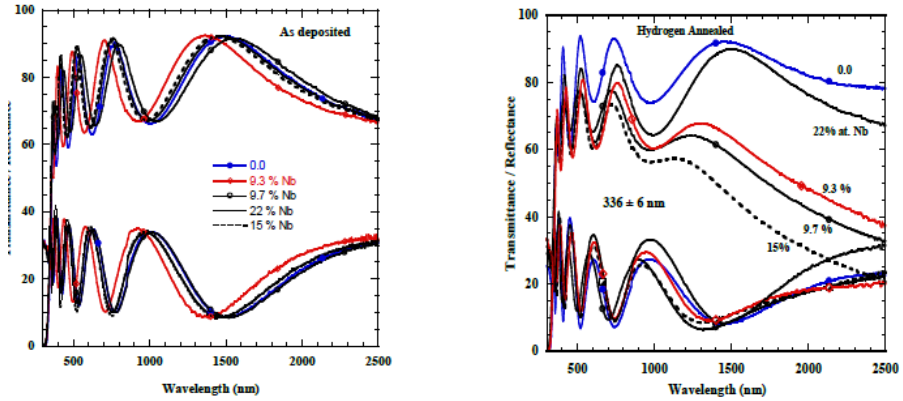

Fig9. *Experimental Spectral Transmittance and Reflectance of undoped and Nb-doped titanium oxide films prepared at 500 ± 15°C before and after post-annealing in Hydrogen atmosphere at 500°C for 1 hour (higher Nb concentrations). Thickness of films was 336 ± 6 nm*

Transmittance and reflectance spectra for the TNO films before and after post annealing for low (Fig) and high Nb concentrations (Fig) demonstrate the high transparency of TNO. The Thickness of films displayed in **Fig** is almost twice those shown in **Fig** for the purpose of amplifying their optical behaviour in the NIR for ease of comparison. Doping transforms the optical properties of the films to a significant degree only after post annealing in hydrogen. Transmittance is approximately 65 - 83% throughout the visible wavelength region. With increasing Nb^{5+} concentration, the transmittance decreased in the wavelength region over 1000 nm. The film with the lowest resistivity had the lowest transmission, especially in the near infrared. According to [[12]], the above can be expected for plasma oscillations of the conduction band electrons in a partially filled d band.

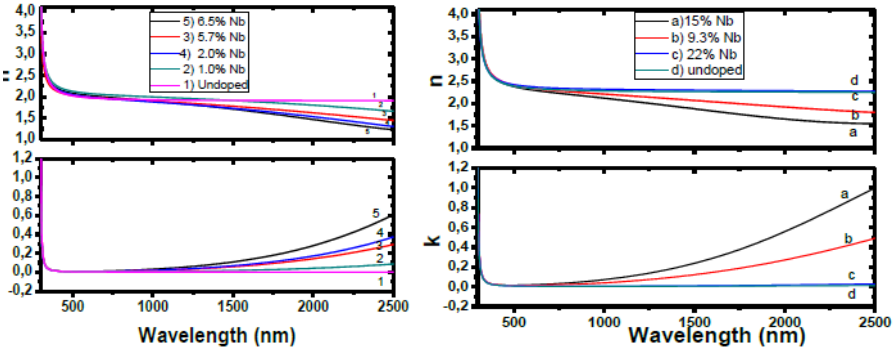

Fig10. *Spectral refractive index and extinction coefficient for* TiO_2 *and* TiO_2 : Nb *films after annealing in 1 atm* H_2 *atmosphere at 500˚C for 1 hour*

The optical constants are reported in Fig showing spectral refractive index n (λ) and extinction coefficient k (λ) for undoped and doped films. The undoped film and the 22 at. % Nb doped film exhibit a dielectric behaviour with n≈2.1 irrespective of wavelength for λ>500 nm. For the Nb doped films, the optical constants are qualitatively different. In this case k(λ) increases for increasing λ, as expected for a metallic material, while n(λ) drops gently towards larger λ. These effects increase in magnitude with increasing doping level of Nb.

The optical band gap, E_g, was determined using the standard formula [[26]].

$$\alpha h\nu \; \alpha \; (h\nu - E_g)^n \qquad \textbf{(8)}$$

Where α=2πk/λ is the absorption coefficient, hν, the photon energy, and n = 2 accounts for the fact that the indirectly

allowed transitions across the band gap are expected to dominate. Fig shows plots of $(\alpha h\nu)^{\frac{1}{2}}$ versus photon energy, $h\nu$, in the high absorption region. Extrapolation of the curve to $h\nu = 0$ gave the indirect band gap of $TiO_2 : Nb$ films in the range 3.38 eV – 3.47 eV for the undoped and heavily doped films; which is comparable with the values already reported [10,14 ,28]. The indirect band gap slightly widens due to the increase in the number of charge carriers with increase in Nb-doping. The direct band gap (n = 1/2) was determined to be 3.75 eV which compares well with 3.8 eV as reported [29].

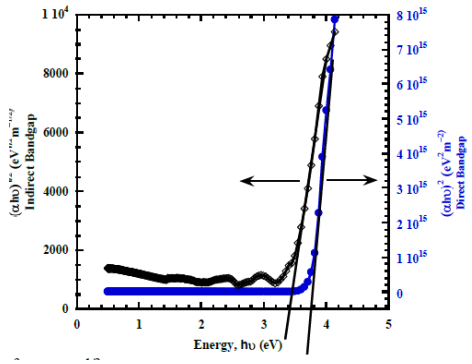

Fig11. $(\alpha h\nu)^{\frac{1}{2}}$ *and* $(\alpha h\nu)^{2}$ *versus* $h\nu$ *plots for determining the optical direct and indirect band gaps of 9.3% Nb-doped titanium oxide films indicated in the figure*

3.4. Electrical Studies

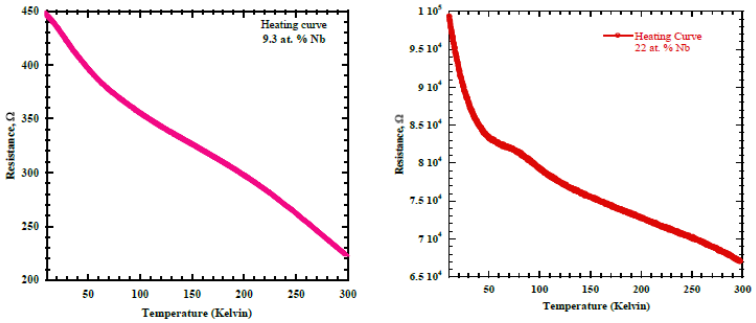

Fig12.*Resistivity variation as a function of temperature for 2 films*

To determine whether the TNO films exhibited metallic behaviour, we measured the resistivity variation with temperature from 10 to 300 K for 9.3%Nb and 2%Nb films and the results are presented in Fig. Surprisingly, the polycrystalline TNO film with room temperature $\rho \sim 10^{-3}$ Ω cm did not exhibit metallic ρ – T behaviour. Instead, the ρ – T curve exhibited semiconducting behaviour. The semiconducting carrier transport with $d\rho/dT < 0$ is a result of the formation of shallow Nb impurity states [4].

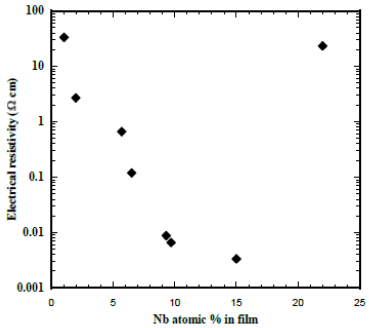

Fig.13.*Variation in electrical resistivity with increasing Nb doping concentration in TiO_2 for Hydrogen annealed films*

The literature values of resistivity variation with temperature from 10 to 300 K of 8 at % Nb doped [10] and 15 at % Nb doped TiO_2 [30] increases with increasing temperature depicting a metallic behavior

Undoped anatase TiO_2 exhibited no measurable conductivity. Nb-doping caused a marked decrease in resistivity, with a minimum values being 3.36×10^{-3} Ωcm at 300 K for 15 at. % Nb as shown in Fig.. Xiao Wan Zheng [Ref 30] has documented a room temperature resistivity of $\sim 1.3 \times 10^{-3}$ Ωcm for 420 nm thick 15 at% Nb doped TiO_2 thin films deposited on (100) $LaAlO_3$ substrates by rf sputtering method.

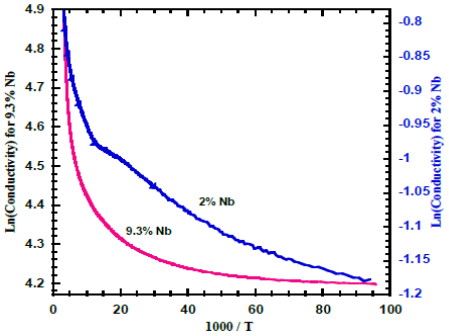

Fig14. *ln σ versus 1/T plots for Nb-doped TiO_2 films.*

The Arrhenius plots of natural logarithm of electrical conductivity, Inσ (*T*), versus reciprocal temperature, 1/*T*, for films having Nb/Ti = 2 and 9.3 in the temperature range from 10 to 300 K is depicted in figure 14. The films clearly do not follow Arrhenius behavior.

Three non distinct regions of σ (*T*) corresponding to the low, intermediate and high temperature ranges are observed. In the high temperature region (190 – 300 K) for 9.3% Nb and (227 - 300 K) for 2% Nb the abrupt increase in σ means that the conduction is thermally activated and assumed to arise from the contribution of the conduction between the extended states. This behaviour of σ (*T*) is well described by the simple Arrhenius law,

$$\sigma(T) = \sigma_0 \exp.\Delta E/K_B T, \qquad (9)$$

Where Δ*E* is the corresponding activation energy and σ_0 the pre-exponential factor. From the slope, the activation energy for TiO_2 was calculated to be ~ 1.0 eV which compares favorably with the value of 0.78 eV as already reported for sprayed undoped TiO_2 films [31]. The calculated values of both Δ*E* and σ_0 are given in Table 1. It is seen that uncertainties in the values of both parameters are high.

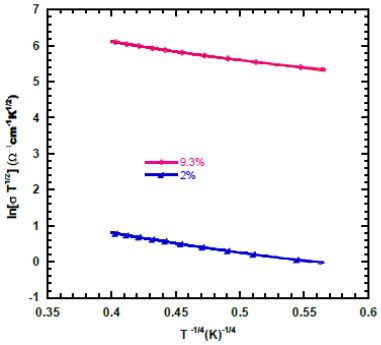

Fig15.*Plots of ln($\sigma T^{1/2}$) versus $(1/T)^{1/4}$ for Nb-doped TiO_2 films.*

The intrinsic electrical conductivity in n-type anatase TiO_2 films has been measured. The value for the band gap E_g was calculated from the experimental data, assuming intrinsic conductivity of the form

$$\sigma = \text{constant} \bullet \text{Exp.}\left(-E_g/2k_B T\right) \qquad (10)$$

We used the intrinsic region in the figure to calculate the band gap of TiO_2 samples. The intrinsic region is the straight line extrapolated with a dashed line.

$$\ell n\,\sigma = -\frac{E_g}{2K_B}\frac{1}{T} + \text{constant} \tag{11}$$

The slope, $-\frac{E_g}{2K_B}$, directly gave the band gap of intrinsic TiO_2 as 2eV which was somewhat narrower than the empirical value of 3.2 eV. This under estimation of the band gap is similar to the one reported for GGA calculations.

We plotted $\ell n(\sigma\sqrt{T})$ versus $(1/T)^{1/4}$ for the low temperature (9.7 - 38.9 K) regime shown in figure 15. The curves are well fitted with straight lines, satisfying Mott's formula for variable range hopping [32]

$$\sigma(T) = \sigma_0'/\sqrt{T}\exp\left[-(T_0/T)^{1/4}\right] \tag{12}$$

Where $T_0 = 16\alpha^3/K_B N(\epsilon_f)$

Rearranging the above equation

$$\ell n\left[\sigma(T)\sqrt{T}\right] = T_0^{1/4}\bullet\frac{1}{T^{1/4}} + \text{constant} \tag{13}$$

Gradient = $T_0^{1/4} = \left[16\alpha^3/K_B N(\epsilon_f)\right]^{1/4}$

σ_0 is the pre-exponential factor, $N(\epsilon_f)$ is the density of localized states at the Fermi level, α describes the spatial extent of the localized wave function and is assumed to be 0.124 $Å^{-1}$ and K_B is the Boltzmann constant. In accordance to Mott's theory, the room temperature hopping distance, R, and hopping energy, W, is given by the following expressions

$$R = \left[9/8\pi\alpha K_B T N(\epsilon_f)\right]^{1/4} \tag{14}$$

$$W = 3/(4\pi R^3 N(\epsilon_f)) \tag{15}$$

Necessary conditions for Mott's variable-range hopping process $W > K_B T$ and $\alpha R >> 1$ are satisfied.

Table1.*Calculated values of ΔE and associated parameters.*

Nb/Ti	ΔE(eV)	σ_0 $(\Omega cm)^{-1}\times10^{-2}$	T_0 (K)	σ_0' $(\Omega cm)^{-1}K^{1/2}$	$N(\epsilon_f)$ $eV^{-1}cm^{-3}\times10^{-25}$	R(cm) $\times10^{9}$	W(MeV) $\times10^{-4}$
2	1.2	1.77	731.16	3007.005	1.9	2.2	1.2
9.3	1.0	0.19	530.84	17.68117	2.6	2.2	1.2

IV. CONCLUSION

Conducting and transparent thin films of Nb doped TiO_2 on Corning 7059 glass substrates were successfully synthesized at $500\pm15^{o}C$ by the low cost, vacuum-free spray pyrolysis technique for the first time. Prior to this, only sputtering and PLD had been used successfully to fabricate highly conducting and transparent TNO films. The Nb-doped TiO_2 films were deposited with do pant concentrations ranging from 0 to 22 at% in the film. The XRD of annealed films showed a polycrystalline anatase (004)-oriented phase without any second phases. ED's studies of chemical composition of the films showed that the exact amounts of Nb in the films are less than that taken in the solution. SEM studies showed that the particle sizes lie in the range 70–300 nm. In the TiO_2 thin films, Nb^{5+} acts as a donor so that, with increasing Nb doping up to 15 at%, the resistivity of the films decreases systematically. However, increase in Nb doping beyond 15 at%, the resistivity increases sharply. The as deposited films were non-conductive but after annealing in H_2 at 1 atm. for 1 hour, doped films turned conductive. Films doped with 15 at.% Nb, 336 nm thick, exhibited a lowest room temperature resistivity of 3.36×10^{-3} Ω cm and visible transmittance of

over 65% after post deposition annealing in H_2. The electrical conductivity increases with the (004) peak intensity which is strongly correlated with the anatase crystallinity. The ρ - T curve for $TiO_2:Nb$ exhibited semiconducting behavior. The optical band gap for undoped and doped films lay in the range 3.38 – 3.47 eV.

V. ACKNOWLEDGEMENTS

The authors would like to thank the International Program in the Physical Sciences (IPPS), Uppsala University for the financial and material support to the Department of Physics, Moi University. Financial support from the Swedish Research Council for this research is greatly appreciated.

REFERENCES

[1] Fujishima A. and Honda K., Nature, 238 (1972) 37

[2] C.G. Granqvist, Transparent conductors as solar energy materials: A panoramic review, Solar Energy Materials & Solar Cells 91 (2007) 1529–1598

[3] Siefering K.L. and Griffin G.L., J. Electrochem. Soc. 137 (1990) 1206.

[4] T. Hitosugi, N. Yamada, S. Nakao and T. Hesegawa, Properties of TiO_2-based transparent conducting oxides, Phys. Status Solidi A 207, No. 7 (2010) 1529-1537.

[5] D. P. Norton, Synthesis and properties of epitaxial electronic oxide thin-film materials, Mater. Sci. and Eng. R 43 (2004) 139–247

[6] Kurtz S. R. and Gordon R. G., Chemical vapor deposition of doped TiO_2, thin films, Thin Solid Films, 147 (1987) 167-176

[7] Mattsson A., Leideborg M., Larsson K., Westin G., and Osterlund L., Adsorption and Solar Light Decomposition of Acetone on Anatase TiO_2 and Niobium Doped TiO_2 thin Films, J. Phys. Chem. B, 110, No. 3 (2006) 1212-1220

A. Tsuzuki, H. Murakami, K. Kani, S. Kawakami, Y. Torii, Preparation of Nb-doped TiO_2 films by Sol-gel method, J. Mater. Sci. Lett. 9 (1990) 624 - 626

[8] Conde-Gallardo A., Guerreroa M., Castillo N., Soto A.B., Fragoso R., Cabanas-Moreno J.G., TiO2 anatase thin films deposited by spray pyrolysis of an aerosol

[9] of titanium diisopropoxide, Thin Solid Films 473 (2005) 68– 73

[10] Y. Sato, Y. Sanno, C. Tasaki, N. Oka, T. Kamiyama, Y. Shigesato, Electrical and optical properties of Nb-doped TiO_2 films deposited by dc magnetron sputtering using slightly reduced Nb-doped TiO_{2-x} ceramic targets, J. Vac. Sci. Technol. A 28(4), (2010) 851–855.

[11] N. Yamada, T. Hitosugi, J. Kasai, N. L. H. Hoang, S. Nakao, Y. Hirose, T. Shimada, T. Hesegawa, Transparent conducting Nb-doped TiO_2 (TNO) thin films sputtered from various targets, Thin Solid Films 518 (2010) 3101–3104

[12] M. A. Gillispie, M. F. A. M. van Hest, M. S. Dabney, J. D. Perkins, and D. S. Ginley, rf magnetron sputter deposition of transparent conducting Nb-doped TiO_2 films on $SrTiO_3$, J. Appl. Phys. 101, (2007) 033125

[13] N. L. H. Hoang, N. Yamada, T. Hitosugi, J. Kasai, S. Nakao, T. Shimada, and T. Hasegawa, Low-temperature Fabrication of Transparent Conducting Anatase Nb-doped TiO_2 Films by Sputtering, Appl. Phys. Express 1 (2008) 115001

[14] C.M. Maghanga, J. Jensen, G.A. Niklasson, C.G. Granqvist and M. Mwamburi, Transparent and conducting $TiO_2:Nb$ films made by sputter deposition: Application to spectrally selective solar reflectors, Solar Energy Materials & Solar Cells 94 (2010) 75–79

[15] T. Hitosugi, A. Ueda, S. Nakao, N. Yamada, Y. Furubayashi, Y. Hirose, S. Konuma, T. Shimada, T. Hasegawa, Transparent conducting properties of anatase $Ti_{0.94}Nb_{0.06}O_2$ polycrystalline films on glass substrate, Thin Solid Films 516 (2008) 5750–5753.

[16] T. Hitosugia, A. Ueda, S. Nakao, N. Yamada, Y. Furubayashi, Y. Hirose, T. Shimada and T. Hasegawa, Fabrication of highly conductive $Ti_{1-x}Nb_xO_2$ polycrystalline films on glass substrates via crystallization of amorphous phase grown by pulsed laser deposition, Appl. Phys. Lett 90, (2007) 212106–3.

[17] T. Hitosugi, A. Ueda, Y. Furubayashi, Y. Hirose, S. Konuma, T. Shimada, and T. Hasegawa, Fabrication of TiO_2-Based Transparent Conducting Oxide Films on Glass by Pulsed Laser Deposition, Jpn. J. Appl. Phys. Vol. 46, No. 3, (2007), pp. L86–L88.

[18] Y. Furubayashi, T. Hitosugi, Y. Yamamoto, K. Inaba, G. Kinoda, Y. Hirose, T. Shimada and T. Hasegawa, A transparent metal: Nb-doped anatase TiO_2, Appl. Phys. Lett. 86, (2005) 252101–3 Y. Furubayashi, T. Hitosugi, Y. Yamamoto, Y.

Hirose, G. Kinoda, K. Inaba, T. Shimada, T. Hasegawa, Novel transparent conducting oxide: Anabas $Ti_{1-x}Nb_xO_2$, Thin Solid Films 496 (2006) 157 – 159.

[19] Karl son T., Roes A. and Ribbing C. G., Influence of spray conditions and do pants on highly conducting tin oxide films, Solar Energy Materials 11 (1985) 469 – 478

[20] L. Kavan and M. Gratzel, Highly efficient semiconducting tio_2, photo electrodes prepared by aerosol pyrolysis, Electrochemical Acta, 40 No. 5 (1995) 643-652

[21] Swinepoxes R. Determination of the thickness and optical constants of amorphous silicon. Phys. E, Sci. In strum. 16, 1214 (1983)

[22] W. Thesis, in: W. Teiss (Ed.), Scout Thin Film Analysis Software Handbook, Hard- and Software, Aachen, Germany, 2001 <www.mtheiss.com>, pp. 54–57.

[23] N. W. Ashcroft, N. D. Mermin, Solid State Physics,, CBS Publishing, Philadelphia, USA, 1976, p. 18.

[24] C.C. Kim, J.W. Garland, H. Abad, P.M. Raccah, Modeling the optical dielectric function of semiconductors: extension of the critical-point parabolic-band approximation, Phys. Rev. B 45 (1992) 11749

[25] J. C. Manifacier, Thin metallic oxides as transparent conductors, Thin Solid Films, 90 (1982) 297 – 308

[26] C.G. Granqvist, Handbook of Inorganic Electrochromic Materials, Elsevier, Amsterdam, the Netherlands, 1995, pp. 265–275.

[27] R. Ayouchi, C. Casteleiro, R. Schwarz, J. R. Barrado, and F. Martín, Optical properties of TiO_2 thin films prepared by chemical spray pyrolysis from aqueous solutions, Phys. Status Solidi C 7, No. 3–4, (2010) 933– 936.

[28] Nickolay Golego, Thin-film polycrystalline titanium-oxygen semiconductors prepared by spray spray pyrolysis, PhD thesis, The University of Guelph, Canada, August 1998.

[29] Xiao Wan Zheng, Zhi Qing Li, (2010) Low-Temperature magnetoresistance of Nb – doped TiO_2 transparent conducting films, Solid State Communications, Vol. 150 PP 1625 – 1628.

[30] Ayouchi R. (2010), C. Casteleiro, R. Schwarz, J.R. Barrado, and F. Martín, Optical properties of TiO2 thin films prepared by chemical spray pyrolysis from aqueous solutions, Phys. Status Solidi C, volume 7, No. 3–4, pp. 933– 936.

[31] Mott, N.F., Conduction in non-crystalline materials, III. Localized states in a pseudo gap and near extremities of conduction and valence bands Phil. Mag. 19: (1969) 835.